

One-point probability distribution function from spherical collapse: Early Dark Energy (EDE) vs. Λ CDM

Ankush Mandal^{1,2*} and Sharvari Nadkarni-Ghosh^{1†}

¹*Department of Physics, I.I.T. Kanpur, Kanpur, U.P. 208016 India*

Email: nsharvari@gmail.com, sharvari@iitk.ac.in

²*Inter-University Centre for Astronomy and Astrophysics, Pune-411007, India*

Email: ankushm@iucaa.in, ankush.contai@gmail.com

ABSTRACT

We compute the one-point PDF of the dark matter density field using the spherical collapse and compare the results to other forms available in the literature, in particular the form given by Bernardeau (B94), the skewed log-normal form (SLN) and the generalized normal distribution version 2 ($\mathcal{N}_{v,2}$). The initial distribution is assumed to be a Gaussian of comoving width σ_G . We consider three cosmological models: the pure matter EdS, the standard Λ CDM and one early dark energy (EDE) model, three values for $\sigma_G : 0.5, 1, 2$ and epochs between $a = 0.1$ to 1. We find that, in overdense regions, the SLN form works best, whereas, in voids B94 and $\mathcal{N}_{v,2}$ are good fits over the entire range of models, scales and epochs considered. We compute the standard deviation of the PDF as a measure of its width and find that, as expected, at late times, the width is lower in EDE than Λ CDM models because of the lower growth rate. We examine the possibility that the width of the PDF, in the quasi-linear regime, can be used as a promising future probe to constrain EDE models. The non-linear growth rate directly depends on the relation between the density and velocity divergence in the non-linear regime. We find that the formula for this relation which was derived for constant w models by Nadkarni-Ghosh also holds true for the EDE model with an accuracy of 3%, thus, increasing its range of validity.

1 INTRODUCTION

The large scale structure observed today is believed to have grown from tiny fluctuations laid down during the inflationary era in the history of the Universe. Observations of the cosmic microwave background suggest that the one-point probability distribution function (PDF) of these primordial fluctuations is very close to a Gaussian (Planck Collaboration¹). At early epochs, when the evolution is linear, the shape of the PDF remains Gaussian and hence symmetric about the origin. However, this symmetry is broken in the non-linear regime. For instance, the density contrast in overdense virialized regions is of the order of a hundred, but it never drops below -1 in void regions, since the total density is always positive. Tracking this (secondary) non-Gaussianity is important because the shape of the PDF carries information about the evolution history and hence can be used to constrain cosmological parameters. While the two-point and higher-order correlation functions give information about the spectral distribution, there is still observational interest in additionally measuring the matter density PDF, either directly in terms of the galaxy counts-in-cell distribution or indirectly through the lensing convergence (Bel et al. 2016; Liu et al. 2016; Patton et al. 2017; Hurtado-Gil et al. 2017; Clerkin et al. 2017; Gruen et al. 2018). This has been shown to provide complementary constraints and help break degeneracies in parameter estimation.

The history of the one-point PDF dates back as early as 1934 when Hubble (1934) examined the frequency distribution of about 44000 galaxies distributed over three-fourth of the sky and found it to be close to log-normal. Following this, there were other many other statistical measures proposed to quantify the departure from Gaussianity, including the extensive work by Neyman (1962) and Scott (1962). A detailed historical summary can be found in Peebles (1980). The early 80s and 90s saw the advent of phenomenological models some of which assumed that gravitational clustering can be described

¹ <https://www.cosmos.esa.int/web/planck>, Planck 2018 results. IX.

by equilibrium thermodynamics (Saslaw & Hamilton 1984; Suto et al. 1990; Lahav et al. 1993). Another phenomenological model which has remained popular till date is the log-normal model proposed by Coles & Jones (1991). This model is partly motivated by the theoretical fact that the full non-linear continuity equation combined with linear statistics for the velocity field, predicts a log-normal statistics for the density field. This form has proven to be a good fit in the quasi-linear regime both theoretically (Kofman 1993; Coles, Melott, & Shandarin 1993; Ohta, Kayo, & Taruya 2003) and observationally (Colombi et al. 2000; Szapudi et al. 2000; Wild et al. 2005; Clerkin et al. 2017). It has also been proposed to fit the weak lensing convergence field Taruya et al. 2002; Hilbert et al. 2011) as well as to predict the void distribution function (Russell & Pycke 2017). However, its validity in the non-linear regime is less established (for e.g., Colombi 1994; Bernardeau & Kofman 1995; Ueda & Yokoyama 1996; Szapudi & Pan 2004; Repp & Szapudi 2018). Recently, Xavier et al. (2016) have also pointed out a mathematical inconsistency in simultaneous modelling the joint distribution of the density and convergence fields and have proposed modifications to the standard form. Numerical simulations have also shown deviations from this form and alternate fitting forms have been proposed (for e.g., Shin et al. 2017; Klypin et al. 2018).

On the theoretical side, analytical modelling of the one-point PDF has been of interest for over three decades. In the 90s, Kofman and Bernardeau and their collaborators used perturbation theory (PT) in the Eulerian and Lagrangian frames to derive the density PDFs and its higher-order moments (Kofman 1993; Kofman et al. 1994; Bernardeau 1994a,b; Bernardeau & Kofman 1995; Colombi et al. 1997). Extensions of this work were done by Fosalba & Gaztanaga (1998) who simplified the higher-order perturbative terms using spherical dynamics so as to apply the formalism to non-Gaussian initial conditions. Juszkiewicz et al. (1995) and Gaztañaga et al. (2000) combined PT with the Edgeworth expansion to get better approximations in the non-linear regime. Taylor & Watts (2000) combined second-order PT with the Chapman-Kolmogorov equation to understand the evolution of the distribution. Estimates based on local dynamics such as spherical and ellipsoidal collapse were given by Ohta et al. (2003, 2004) who formulated the differential equations for the evolution of the one-point PDFs as well as Lam & Sheth (2008a,b) who used excursion sets to construct the PDF in both real and redshift space.

One non-perturbative approach was put forth by Valageas who recast the solution to the collisionless Boltzmann equation as path integral to be solved within the saddle-point approximation using the method of steepest descent. The dynamics near the saddle point depends only on the scale separation because of the homogeneity and isotropy of the Universe and spherical symmetry is invoked to provide a unique mapping between the initial linear state and the final non-linear state of the system (Valageas 1998, 2001, 2002a,b,c,d; Valageas & Munshi 2004). This was further developed and applied to compute the statistic of density profiles by Bernardeau et al. (2014, 2015). Very recently, Ivanov et al. (2019) have extended this calculation to compute the effect of fluctuations around the spherical saddle point, which they argue is necessary for the consistency of the theory. Bernardeau & Reimberg (2016) have recently proposed another non-perturbative approach that uses Large Deviations Theory to compute the cumulant generating functions. This approach also relies on having a unique mapping between initial and final densities given by local approximations like spherical or cylindrical collapse (Uhlemann et al. 2016, 2018). This method has been applied to a variety of problems: to compute marginal and joint density and velocity-divergence PDFs (Uhlemann et al. 2017), the weak lensing convergence PDF (Reimberg & Bernardeau 2018) and to constrain dark energy models (Codis et al. 2016).

Many of the above theoretical methods use spherical collapse dynamics as a proxy for the non-linear regime. The main advantage is that the equations are simple second-order ordinary differential equations (ODEs). Analytic solutions are available for pure matter cosmologies and numerical solutions can be easily generated not only for Λ CDM but also for many other non-standard cosmological models such as those with a constant equation of state ($w \neq -1$) or those with a time-varying w . The exceptions are cases where dark matter and dark energy are coupled or Einstein's law of gravity is modified since these systems are higher-order with additional perturbation variables. In spite of this simplicity, most of the aforementioned investigations that invoke spherical dynamics have been restricted to pure matter or Λ CDM only.

In this paper, we use the spherical collapse model to compute the one-point PDF and compare the case of an Early Dark Energy (EDE) model with the usual Λ CDM cosmology. The physical assumption is that each spatial point evolves independently (local approximation) as if it were an isolated spherical perturbation in an expanding background cosmology. The stochasticity is in the initial conditions: they are drawn from a random Gaussian distribution. This paper has two primary aims. First, we want to check how well the non-linear PDF from spherical collapse compares with other fitting forms in the literature and second, we want to understand the effect of early dark energy on structure, in particular on the one-point PDF. Nadkarni-Ghosh (2013) also considered spherical collapse to obtain the density-velocity divergence relation (DVDR) in the non-linear regime. However, the investigation was restricted to dark energy models with constant equation of state (w). A third, tertiary aim of this work is to also check if the fitting form for the non-linear DVDR obtained in N13 also works for the EDE model with a time-varying w .

The paper is organized as follows. §2 sets up the equations for non-linear evolution of the density field for spherically symmetric perturbations expanding in a background cosmology consisting of a dark energy component that neither clusters nor couples to the matter component. §3 discusses the growth rates in the linear and non-linear regime and compares the behaviour of the EDE model with the standard Λ CDM model. Here we also check how well the non-linear DVDR relation obtained in N13 works for the EDE model by comparing the theoretical and numerical non-linear growth rates. §4 gives

the details of the numerical runs performed to generate the PDF and compares the results to fitting forms existing in the literature. We consider three forms: the theoretical prediction based on perturbation theory (Bernardeau 1994a), the skewed log-normal (Colombi 1994) and the generalized normal distribution, version 2 (Shin et al. 2017). §5 investigates whether the standard deviation and higher-order moments of the PDF can be used as a probe to discriminate between EDE and Λ CDM. We conclude in §6.

2 THE PHYSICAL SET-UP

2.1 Non-linear evolution equations in the Spherical Collapse (SC) model

The physical system is a constant density (top-hat) sphere, evolving in a homogenous and isotropic, flat background universe consisting of pressureless matter and dark energy with equation of state w , which may vary with time. Matter is allowed to cluster whereas dark energy is assumed to be uniform, and non-interacting with the matter sector. For such cosmologies, the scale factor a of the background evolves as

$$H^2 = H_0^2 \left[\frac{\Omega_{m,0} a_0^3}{a^3} + \Omega_{de,0} \exp \left\{ -3 \int_{a_0}^a (1 + w(y)) \frac{dy}{y} \right\} \right], \quad (1)$$

where $H = \dot{a}/a$. The ‘dot’ denotes derivative with respect to coordinate time, y is the dummy variable used for the integral and a_0 is the value of the scale factor today, usually set to 1. The matter and dark energy parameters are denoted as Ω_m and Ω_{de} respectively and the subscript ‘0’ denotes their values today. Using the conservation of energy density, the density parameters at any epoch are related to their values today as

$$\Omega_m(a) = \frac{H_0^2 a_0^3 \Omega_{m,0}}{H^2 a^3} \quad (2)$$

$$\Omega_{de}(a) = \frac{H_0^2}{H^2} \Omega_{de,0} \exp \left\{ -3 \int_{a_0}^a (1 + w(y)) \frac{dy}{y} \right\} \quad (3)$$

For a flat universe, $\Omega_m(a) + \Omega_{de}(a) = 1$ for all epochs. Let the origin be at the center of the spherical perturbation and let \mathbf{r} and \mathbf{x} be the physical and comoving radius of the outer edge. The perturbed sphere may be surrounded by a compensating region, which is either a mass shell or a void, depending upon whether the perturbation is underdense or overdense with respect to the background. Let $\bar{\rho}_m$ and ρ_m be the density of the background and perturbation respectively. For the dark energy models considered in this paper, an initial top-hat stays a top-hat and the dynamics can be solely described by two purely time-dependent quantities: fractional overdensity (δ) and the scaled divergence of the peculiar velocity (Θ) defined as

$$\delta = \frac{\rho_m}{\bar{\rho}_m} - 1, \quad (4)$$

$$\Theta = \frac{1}{H} \nabla_r \cdot \mathbf{v}, \quad (5)$$

where $\bar{\rho}_m$ and ρ_m are the densities of the background and perturbation respectively and $\mathbf{v} = \dot{\mathbf{r}} - H\mathbf{r} = a\dot{\mathbf{x}}$ is the peculiar velocity. For a pure matter cosmology, it is possible to invoke Birkoff’s theorem and treat the perturbed sphere as a separate universe whose evolution is dictated by an equation analogous to eq. (1), with a different scale factor and density parameter. However, extensions to dark energy cosmologies are not obvious. Here we adopt the approach of starting with the hydrodynamic equations: the generalized continuity and Euler equations along with the Poisson equation for the gravitational potential (Lima et al. 1997; Abramo et al. 2009; Pace et al. 2010, 2017). These are valid for general non-interacting dark energy cosmologies, in the sub-horizon limit and in the absence of shell-crossing. The resulting equations for δ and Θ are

$$\delta' = -(1 + \delta)\Theta \quad (6)$$

$$\Theta' = -\frac{3}{2}\Omega_m(a)\delta - \Theta \left(2 + \frac{H'}{H} \right) - \frac{\Theta^2}{3}. \quad (7)$$

The prime denotes derivative with respect to $\ln a$. The details of the derivation are in appendix A. Combining eq. (6) and eq. (7) gives one second order equation for the non-linear evolution of δ .

$$\delta'' + \left(2 + \frac{H'}{H} \right) \delta' - \frac{4}{3} \frac{\delta'^2}{(1 + \delta)} - \frac{3}{2} \Omega_m(a) \delta (1 + \delta) = 0. \quad (8)$$

For the flat dark energy models, with varying equation of state, eq. (8) reduces to

$$\delta'' + \frac{1}{2} [1 - 3w(a)\Omega_{de}(a)] \delta' - \frac{4}{3} \frac{\delta'^2}{(1 + \delta)} - \frac{3}{2} \Omega_m(a) \delta (1 + \delta) = 0. \quad (9)$$

This system is also valid if the density has a radial variation: in that case δ has to be replaced by its spherically averaged value (N13).

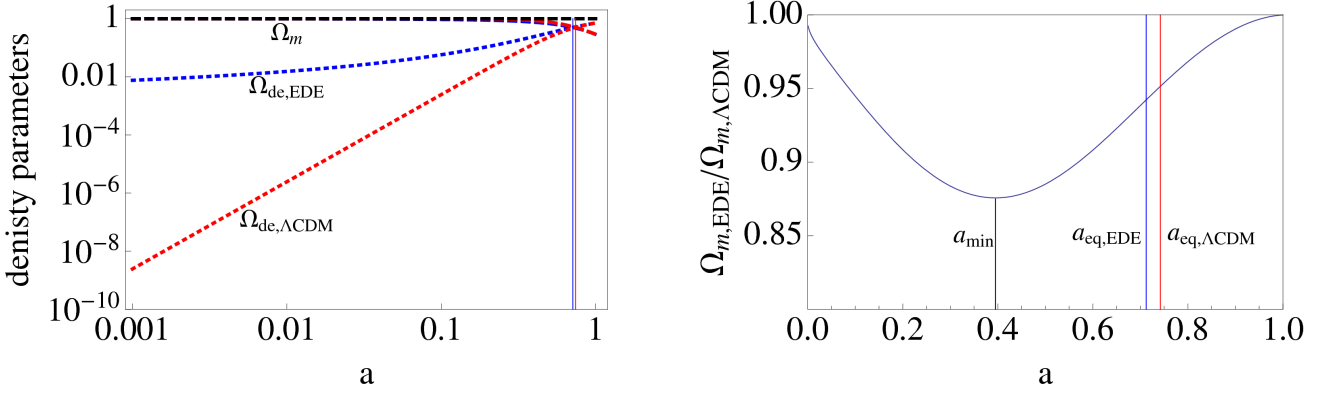


Figure 1. Evolution of density parameters. Left panel: the matter density parameter is unity for the EdS cosmology. The EDE model has a non-negligible contribution at early epochs as compared to Λ CDM, but the Ω_m is still close to unity for both models. Right panel: the ratio of the matter density parameters in EDE relative to the Λ CDM cosmology. The ratio is minimum around $a \sim 0.4$. The vertical blue and red lines in both panels indicate the epoch of matter-dark energy equality for EDE and Λ CDM respectively. They are very close and almost indistinguishable on a log-axis.

2.2 Initial conditions

Equation (9) can be completely solved by specifying δ and δ' at some initial time a_i . From eq. (6), we have $\delta'_i = -(1 + \delta_i)\Theta_i$. In principle, δ_i and Θ_i are independent however, usually cosmological initial conditions assume the Zeldovich approximation (Zeldovich 1970). This states that the velocity field is proportional to the acceleration field; the proportionality constant is chosen so as to ensure that there are no perturbations at the big bang time. In linear, Eulerian perturbation theory, for the EdS cosmology, this is equivalent to setting the coefficient of the decaying mode to zero and the growing mode solution is $\delta(a) \propto a$, which gives $\delta' = \delta$ or $\Theta = -\delta$. In this paper, we use the generalization given by Linder (2005) for dark energy cosmologies: $\Theta_i = \Omega_{m,i}^{0.55} \delta_i$. For sufficiently early epochs and sufficiently small δ_i , this reduces to $\delta'_i = \delta_i$. We will discuss extensions of this linear relation in §3.

2.3 Cosmological models

In this paper, we consider three different cosmologies: (a) EdS i.e., $\Omega_{m,0} = 1$, $\Omega_{de,0} = 0$, (b) Λ CDM with $\Omega_{m,0} = 0.29$, $\Omega_{de,0} = 0.71$, (c) Early Dark Energy (EDE hereafter) model with varying equation of state

$$w(a) = \frac{w_0}{(1 + by)^2} \quad (10)$$

with

$$b = -\frac{3w_0}{\ln\left(\frac{1-\Omega_{de,e}}{\Omega_{de,e}}\right) + \ln\left(\frac{1-\Omega_{m,0}}{\Omega_{m,0}}\right)}, \quad (11)$$

where $\Omega_{de,e}$ is the value of Ω_{de} at very early time ($a \rightarrow 0$), w_0 is the value of equation of state parameter at present day and $y = -\ln a$. This three-parameter model was first proposed by Wetterich (2004) and later also considered by Doran & Robbers (2006). In this paper, we set $\Omega_{de,e} = 8 \times 10^{-4}$ and $w_0 = -0.99$. The value for $\Omega_{m,0}$ was chosen to be the same as the Λ CDM model and flatness sets $\Omega_{de,0}$. A similar choice (with slightly different values for the density parameters today) was made by Grossi & Springel (2008) who investigated the effect of such models on non-linear large scale structure. An alternative approach is to consider the best fit values for an EDE cosmology, which in general will be different than those in Λ CDM Jennings et al. (2010), but we do not adopt this approach here. We do not consider a larger range of EDE models because the main aim is to qualitatively contrast the growth of the PDF in Λ CDM and EDE scenarios.

Figure 1 shows the evolution of the matter density for the three models considered in this paper. The left panel shows the density parameters Ω_m and Ω_{de} in all three cosmologies. The EDE cosmology has a non-negligible amount of dark energy at early times. Assuming flatness this amounts to a lower value of Ω_m at early epochs. The EdS cosmology has $\Omega_m = 1$ at all epochs. The right panel shows the ratio of the matter density parameters for the dark energy cosmologies: $\Omega_{m,EDE}/\Omega_{m,\Lambda\text{CDM}}$. The ratio is minimum at around $a \sim 0.4$. The difference in growth rates between the two models is sensitive to this ratio; see figure 3.

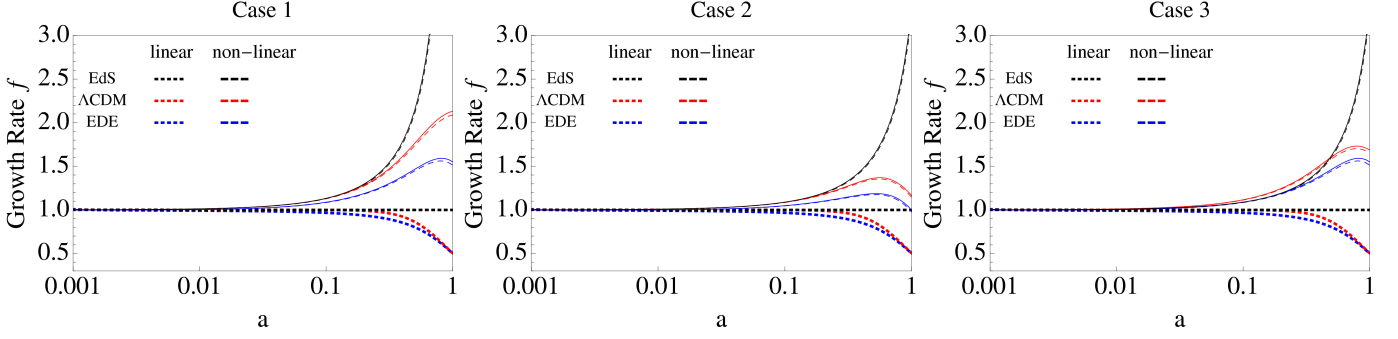


Figure 2. The linear and non-linear growth rates for the three cases discussed in the text. EDE models have a slower growth rate than Λ CDM in both the linear and non-linear regimes. At $a = 1$, the models have the same Ω_m and hence the linear growth rate is the same at that epoch. The EdS model is plotted for reference. The difference between the growth rates is more pronounced in case 1 (where the amplitudes are the same for all three models) than in case 3 (where the EDE amplitude is greater than the Λ CDM amplitude). They are also more pronounced in case 1 compared to case 2 since the latter has a lower amplitude than in case 1; the amplitude is the same for all three models.

3 LINEAR AND NON-LINEAR GROWTH RATES

The non-linear evolution of δ in the SC model is given by eq. (9). The growth rate f is defined as

$$f = \frac{d \ln \delta}{d \ln a}. \quad (12)$$

In the linear regime, f is independent of δ , whereas in the non-linear regime it is a function of δ . The higher the δ , the higher the growth rate. Using the continuity equation (eq. (6)), f can also be expressed as

$$f = -\frac{1 + \delta}{\delta} \Theta. \quad (13)$$

Thus, knowing the relation between the δ and Θ , it is possible to compute the growth rate as a function of density. This relation has been studied extensively by various authors in the past, using perturbation theory (e.g., Bernardeau 1992) or numerical simulations. Bilicki & Chodorowski (2008) gave a fit based on analytical solutions of SC. N13, investigated the w dependence of this relation, also using SC, but without relying on the analytic solutions. The main idea was to impose the condition that there be ‘no perturbations at the big bang’. This is a generalization of the idea of ‘no decaying mode’, which is the basis of the ‘Zeldovich approximation’. This condition imposes a unique relation between δ and Θ , which traces out a curve in the two dimensional $\delta - \Theta$ phase space, called the ‘Zeldovich curve’². By examining the dynamics of the perturbations in the $\delta - \Theta$ phase-space, it was shown that the Zeldovich curve is special: perturbations that start on it, stay on it and others converge to it. It forms an invariant set of the dynamical system defined by eq. (6) and (7) and it corresponds to the late time (non-linear) density velocity-divergence relation (DVDR). N13 obtained a fitting form based constant w cosmologies:

$$\Theta_{fit}(\Omega_m, w, \delta) = \begin{cases} 3A(\Omega_m, w) \left(1 - (1 + \delta)^{B(\Omega_m, w)}\right), & -1 \leq \delta \leq 1 \\ 3\Omega_m^{\gamma_1(w) + \gamma_2(w)} \left[(1 + \delta)^{1/6} - (1 + \delta)^{1/2}\right], & 1 \leq \delta \leq 10 \end{cases} \quad (14)$$

where

$$A(\Omega_m, w) = \frac{1}{2}\Omega_m^{\gamma_1(w)}, \quad B(\Omega_m, w) = \frac{2}{3}\Omega_m^{\gamma_2(w)}, \quad \gamma_1(w) = -0.56(-w)^{-0.08} \quad \text{and} \quad \gamma_2(w) = -0.01(-w)^{-1.18}. \quad (15)$$

Here Ω_m is evaluated at the epoch of interest. This fit is an extension of the forms given by Bernardeau (1992) and Bilicki & Chodorowski (2008). Here we check the validity of this form for EDE models.

Substituting from eq. (14) gives

$$f_{fit}(\Omega_m, w, \delta) = \begin{cases} -3A(\Omega_m, w)\delta^{-1} \left((1 + \delta) - (1 + \delta)^{B(\Omega_m, w) + 1} \right), & -1 \leq \delta \leq 1 \\ -3\Omega_m^{\gamma_1(w) + \gamma_2(w)}\delta^{-1} \left[(1 + \delta)^{7/6} - (1 + \delta)^{3/2} \right], & 1 \leq \delta \leq 10 \end{cases} \quad (16)$$

where, A and B are evaluated using eq. (15). We compare this form to the numerically computed growth factor obtained by solving eq. (9) for Zeldovich initial conditions. We consider three cases:

- Case 1: $\delta = 1.44 \times 10^{-3}$ at $a = 0.001$ for all three cosmologies.

² In N13, δ_v was used instead of Θ ; $\Theta = 3\delta_v$.

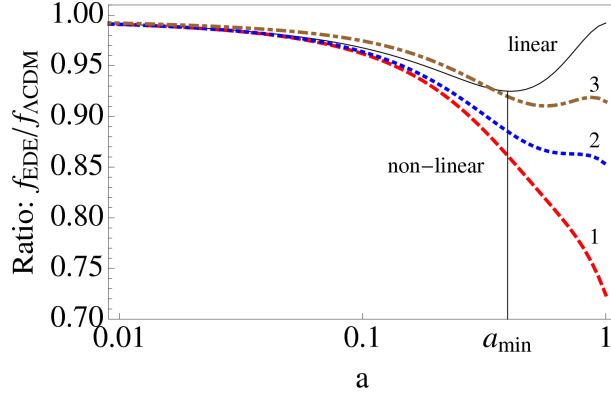


Figure 3. Ratio of the linear and non-linear growth rates between the EDE and Λ CDM models. The ratio of the linear growth rates is independent of the initial conditions since it depends only on the cosmological parameters. The ratio is minimum near $a_{min} \sim 0.4$, which is where the ratio of matter density parameters is minimum; the slight offset indicates a weak dependence on the equation of state w .

- Case 2: $\delta = 1 \times 10^{-3}$ at $a = 0.001$ for all three cosmologies.
- Case 3: $\delta_L = 1$ at $a = 1$ for all three cosmologies, where δ_L is the linearly evolved amplitude. Multiplying by the appropriate linear growth factor gives $\delta = 1.44 \times 10^{-3}$, 1.29×10^{-3} and 1×10^{-3} at $a = 0.001$ for EDE, Λ CDM and EdS cosmologies respectively.

Figure 2 shows the resulting growth rates for the three cases. The blue, red and black lines indicate EDE, Λ CDM and EdS cosmologies respectively. The dotted and dashed lines are the linear and non-linear growth rates computed numerically. The solid lines indicate the fits given by eq. (16), where δ is evaluated using the numerical solution. We found that over the full range of epochs considered here, the maximum relative error between the numerical value and the value given by the fit was less than 3 %, indicating that the form given by eq. (16) also works well for the EDE model considered here.

In the linear regime, the fitting function reduces to

$$f_{lin,fit}(\Omega_m, w) = \Omega_m^{\gamma_1(w) + \gamma_2(w)}. \quad (17)$$

For the Λ CDM value, it agrees with the commonly used parametrization of Linder (2005)

$$f_{Linder} \approx \Omega_m^{0.55}. \quad (18)$$

The linear growth rate depends only on the cosmological parameters and it remains unchanged in the three cases. For an EdS cosmology, δ is proportional to the scale factor a and hence the linear growth rate is unity. The non-linear growth rate depends on (a) the instantaneous value of δ , which depends on the initial amplitude and (b) the cosmological density parameters. The EDE and Λ CDM cosmologies have growth rates lower than EdS, both in the linear and non-linear regime, due to the difference in Ω_m between these cosmologies. The initial amplitude in case 1 was higher than in case 2. Thus, for all three cosmologies, the growth rate is higher in case 1 and also higher in Λ CDM than EDE as expected. In case 3, the linear amplitude at $a = 1$ was in all the three cosmologies was fixed to be unity. This implies a lower initial amplitude in Λ CDM than in the EDE cosmology. The higher value of Ω_m in the Λ CDM case still gives a higher non-linear growth rate as compared to EDE, but the differences are less pronounced than in case 1. The effect of a lower initial amplitude is partially compensated by a higher Ω_m .

From the fitting functions, it is clear that the dependence on w is very weak, even in the non-linear regime. In the linear regime, it is usually neglected to give $f_{lin} \sim \Omega_m^{0.55}$ for most dark energy cosmologies with standard gravity i.e., w is assumed to be -1. We found that, for the EDE cosmology, using the fitting functions with $w = -1$ as opposed to the correct value of w gave only an error of 0.8% (0.4%) in the non-linear (linear) growth rate. This indicates that the difference in growth rates between Λ CDM and EDE cosmology is primarily from the Ω_m dependence. Figure 3 shows the ratio of the growth rates in the EDE to the Λ CDM cosmology. The black solid line is the ratio in the linear regimes and the dashed, dotted and dot-dashed show the ratio in the non-linear regime for the three cases discussed above. The black vertical line indicates the position where the ratio $\Omega_{m,EDE}/\Omega_{m,\Lambda CDM}$ is minimum i.e., $a \sim 0.4$. The ratio of the linear growth rates also reaches its minimum close to $a \sim 0.4$.

4 ONE-POINT PDF OF THE DENSITY FIELD

4.1 Numerical Runs

Numerical runs were performed for an ensemble of initial conditions drawn from a Gaussian random field with mean 0 and standard deviation σ_G . Three values were considered: $\sigma_G = 0.5, 1$ and 2 . For a BBKS power spectrum with $n_s = 1$ and $\sigma_8 = 0.9$, this corresponds roughly to $15, 7$ and $3 h^{-1}$ Mpc. σ_G is the width of the PDF at $a = 1$. The linearly scaled Gaussian at any epoch has the width

$$\sigma_L(a) = \sigma_G \frac{D_1(a)}{D_1(a=1)}, \quad (19)$$

where $D_1(a)$ is the linear growth factor (Dodelson 2003, chapter 7). For each value of σ_G , we considered five realizations each containing 5×10^4 points. The realizations at $a = 1$ are the same for all three cosmologies; to get the initial conditions at $a = a_i$ it is necessary to multiply by the correct linear growth factor. The initial time was $a_i = 0.001$ and final densities were read out at $a = 0.1, 0.4$ and 1 corresponding to redshifts of $z = 9, 1.5$ and 0 respectively. For the PDF analysis, the data cut-off was imposed at $\delta \leq 5$ and we chose 40 bins, equispaced on the log-scale. The PDF is the average over five realizations and error bars correspond to the standard deviation.

4.2 Fitting forms for comparison

In this paper, we have considered three fitting forms (1) the distribution based on Eulerian perturbation theory given by Bernardeau (1994a); hereafter referred to as the B94 distribution, (2) the skewed log-normal distribution (SLN) which combines the Edgeworth series and the log-normal form (Colombi 1994) and (3) the generalized normal distribution ($\mathcal{N}_{\nu 2}$) based on numerical simulations given by (Shin et al. 2017). We compare the analytic expressions to the PDF generated from our numerical runs.

Estimates based on Eulerian Perturbation Theory

The B94 is a piecewise distribution for density field and given by,

$$P(\delta) = \begin{cases} P_{B94}^I(\delta) & -1 \leq \delta < 0.3 \\ P_{B94}^{II}(\delta) & \delta > 0.3, \end{cases} \quad (20)$$

where

$$P_{B94}^I(\delta)d\delta = \left(\frac{7 - 5(1 + \delta)^{\frac{2}{3}}}{4\pi\sigma_\delta^2} \right)^{\frac{1}{2}} (1 + \delta)^{-\frac{5}{3}} \exp \left[-\frac{9}{8\sigma_\delta^2} \left(-1 + \frac{1}{(1 + \delta)^{\frac{2}{3}}} \right)^2 \right] d\delta \quad (21)$$

$$P_{B94}^{II}(\delta)d\delta = f_c \frac{3a_{s\delta}\sigma_\delta}{4\sqrt{\pi}} (1 + \delta)^{-\frac{5}{2}} \exp \left[\frac{-|y_{s\delta}|\delta + |\phi_{s\delta}|}{\sigma_\delta^2} \right] d\delta, \quad (22)$$

where $\sigma_\delta = \sigma_L$, where σ_L is given by eq. (19), $a_{s\delta} = 1.84$, $y_{s\delta} = -0.184$, $\phi_{s\delta} = -0.03$. We have chosen the $n = -3$ values for the parameters a_s, y_s, ϕ_s (B94). The correction factor f_c is

$$f_c = [1 + 2(0.8 - \sigma_\delta)\sigma_\delta^{-1.3}(1 + \delta)^{-0.5}] \quad (23)$$

accounts for the fact that the PDF based on perturbation theory does not perform well at high δ .

The B94 distribution is derived in the Eulerian frame. The estimates of the PDF based on spherical dynamics are in the Lagrangian frame since the mass of the sphere stays constant and the change in density is due to a change in volume. The two are related as (see Bernardeau 1994a; Nadkarni-Ghosh & Singhal 2016, appendix E)

$$P_E(\delta) = \frac{P_L(\delta)}{1 + \delta}, \quad (24)$$

where $P_E(\delta)$ and $P_L(\delta)$ are the PDFs in Eulerian and Lagrangian frame, respectively.

Skewed log-normal distribution (SLN)

The skewed log-normal PDF (P_{SLN}) proposed by Colombi (1994) combines the log-normal PDF and the Edgeworth series. Define $\nu \equiv \Phi/\sigma_\Phi$, with $\Phi \equiv \ln(1 + \delta) - \langle \ln(1 + \delta) \rangle$, $\sigma_\Phi \equiv \sqrt{\langle \Phi^2 \rangle}$, where the brackets denote the average over the ϕ values. P_{SLN} , which uses the third order Edgeworth expansion, is defined as

$$P_{SLN}(\nu)d\nu = \left[1 + \frac{1}{3!}T_3\sigma_\Phi H_3(\nu) + \frac{1}{4!}T_4\sigma_\Phi^2 H_4(\nu) + \frac{10}{6!}T_3^2\sigma_\Phi^2 H_6(\nu) \right] \mathcal{N}(\nu), \quad (25)$$

where

$$T_3 \equiv \frac{\langle \Phi^3 \rangle}{\sigma_\Phi^4}, \quad (26)$$

$$T_4 \equiv \frac{\langle \Phi^4 \rangle - 3\sigma_\Phi^4}{\sigma_\Phi^6}, \quad (27)$$

$$\mathcal{N}(\nu) = \frac{1}{\sqrt{2\pi}} \exp\left[-\frac{\nu^2}{2}\right] \quad (28)$$

and $H_m(\nu)$ is the Hermite polynomial of degree m . This distribution is not always positive definite, i.e., it can be negative valued hence is not a real PDF (Colombi 1994). But, N-body simulations show that this approximation successfully describes the late-time evolution of the dark matter field (Ueda & Yokoyama 1996; Szapudi & Pan 2004).

Generalised normal distribution of version 2 (\mathcal{N}_{v2})

This distribution has been recently proposed by Shin et al. (2017) based on numerical simulations of five different cosmological models. The \mathcal{N}_{v2} distribution consists of three parameters namely, α (scale), κ (shape) and ξ (location). α is related to the width of the distribution, κ quantifies skewness and ξ gives the location of the peak. In terms of these parameters, the \mathcal{N}_{v2} is defined as,

$$\mathcal{N}_{v2}(\delta) = \frac{\mathcal{N}(y)}{\alpha - \kappa(\delta - \xi)}, \quad (29)$$

where $\mathcal{N}(y)$ is the usual Gaussian distribution with mean 0 and variance 1. Here y is defined as,

$$y = \begin{cases} -\frac{1}{\kappa} \ln \left[1 - \frac{\kappa(\delta - \xi)}{\alpha} \right], & \text{if } \kappa \neq 0 \\ \frac{\delta - \xi}{\alpha}, & \text{if } \kappa = 0, \end{cases} \quad (30)$$

A positive (or negative) value of κ yields a left-skewed (or right-skewed) distribution bounded to the right (or left). The mean (μ), median ($\tilde{\delta}$) and skewness (γ_1) of the distribution are related to α , κ and ξ as

$$\mu = \langle \delta \rangle = \xi - \frac{\alpha}{\kappa} \left(e^{\kappa^2/2} - 1 \right) \quad (31)$$

$$\tilde{\delta} = \xi \quad (32)$$

$$\gamma_1 = \frac{\langle (\delta - \mu)^3 \rangle}{(\langle (\delta - \mu)^2 \rangle)^{3/2}} = \frac{3e^{\kappa^2} - e^{3\kappa^2} + 2}{(e^{\kappa^2} - 1)^{3/2}} \text{sign}(\kappa). \quad (33)$$

Here the ' $\langle \cdot \rangle$ ' denotes average over the domain of δ . \mathcal{N}_{v2} approaches the usual Gaussian normal distribution in the limit that κ tends to zero. In this case, $\mu = \xi$ and $\gamma_1 = 0$. There are two ways to find the parameters α , κ and ξ . One way is to compute μ , $\tilde{\delta}$ and γ_1 from the data and solve eqs. (31), (32) and (33) for the three parameters. The other way is to find the best fit values by optimizing the fit to the data. We implemented the latter method using Python's SciPy inbuilt function. This method requires an initial guess for α , κ and ξ . We found that the errors were minimum when the initial guess values were computed analytically using the first method. Table B1 in appendix B shows the values of parameters for the best fit.

4.3 Results and discussion

We compute the numerical one-point PDF as described in §4.1 and compare it with the fitting forms described above. The shape of the PDF evolves with time and depends upon σ_G . Figure 4 shows the variation of the PDFs with epoch for fixed σ_G and figure 5 shows the dependence on σ_G for a fixed epoch for the Λ CDM and EDE cosmologies. At $a = 0.1$, the evolution is still approximately linear and the width is given by σ_L . Non-Gaussianity sets in at later epochs: the width of the PDF increases with increasing epoch for a given σ_G and increases with σ_G at a given epoch. There are no differences between the EDE and Λ CDM cosmologies that are appreciable by eye; we will quantify the evolution of the width for the two cosmologies in the next section.

In order to understand which form fits the best, we calculate the percentage error for the numerical PDFs with respect to each analytic form. Let $P_{sc}(a, \sigma_G, \delta)$ denote numerical PDFs derived from SC and $P_{ana}(a, \sigma_G, \delta)$ be the fitting form. The

error between the two functions is defined as

$$\varepsilon_{rms}(a, \sigma_G) = \sqrt{\frac{1}{N} \sum_{k=1}^N |\varepsilon(a, \sigma_G, \delta_k)|^2}, \quad (34)$$

$$\text{where } \varepsilon(a, \sigma_G, \delta_k) = \frac{P_{ana}(a, \sigma_G, \delta_k) - P_{sc}(a, \sigma_G, \delta_k)}{P_{ana}(a, \sigma_G, \delta_k)}, \quad (35)$$

where N is the number of bins and δ_k is the mean value of the k -th bin. The δ range is divided into two regions: under-dense ($\delta < 0$) and over-dense ($0 \leq \delta < 5$) and the error is calculated separately in each region for each analytic form. The error for the three cosmological models is tabulated in table C1 appendix C. Table C2 gives the error variation with epoch (averaged over σ_G) and table C3 gives the error variation with σ_G (averaged over epoch). The general trends are:

- In overdense regions, SLN provided the best overall fit for all the three models. The error ε_{rms} , averaged over the entire range of epochs, scales and cosmologies was about 11 %, whereas it was 22 % for \mathcal{N}_{v2} and about 33 % for B94. The maximum error for SLN over the entire range was 23%.
- In underdense regions, \mathcal{N}_{v2} and B94, both perform similarly when averaged over epochs, scales and cosmologies. The average error is 35 %, significantly higher than that for overdense regions. Comparing the distributions for individual cosmologies, we find that for EDE cosmology, in particular, the \mathcal{N}_{v2} function fits the data significantly better than B94. This may be just a coincidence since this trend is not observed for either EdS or Λ CDM. It is not surprising that SLN does not fit the void regions very well, because the Edgeworth series starts to breakdown in this regime (see Colombi 1994, figure 1).
- We expect that the fits are better for smaller values of σ_G and earlier epochs. This is seen when the errors are averaged over σ_G for a fixed epoch and averaged over epoch for a fixed σ_G .

The SC model is a local model, i.e., each perturbation is assumed to evolve independently. It does not account for tidal forces which cause shear, rotation and accretion. It also ignores non-linear mode coupling, which is a non-local effect. Yet, it recovers the shape of the PDF given by perturbative methods and simulations reasonably well, over a wide range of epochs, scales and cosmologies. The SC model has been successful in other contexts as well. The non-linear relation between the density and velocity field obtained by simulations is a scatter plot, but the ‘mean’ relation is well described by the SC model (Bernardeau et al. 1999; Kudlicki et al. 2000; Bilicki & Chodorowski 2008). It has also been successfully used to treat the shell crossing regime in Lagrangian perturbation theory Kitaura & Heß (2013). Some of this success can be attributed to a partial cancellation between various effects that have been neglected. One illustration of this feature is to consider the effect of rotation and shear. Both terms appear in the Raychaudhuri equation, which dictates the evolution of Θ and consequently the full non-linear evolution of δ . But they appear with opposite signs (Peebles 1980). Spherical symmetry ignores both terms, giving rise to a partial cancellation. For example, in modelling the non-linear DVDR, the result of simulations agree better with spherical collapse rather than ellipsoidal collapse (Nadkarni-Ghosh & Singhal 2016). This is because ellipsoidal dynamics accounts for only for the shear and does not benefit from the partial cancellation. These arguments are akin to reasons ‘why the Press- Schechter formalism works so well’ (Monaco 1999).

5 WIDTH OF THE ONE-POINT PDF

Many past investigations have looked at the effect of an early dark energy component on the non-linear growth of structure, particularly for the type of EDE model considered here. Bartelmann et al. (2006) considered the SC model and computed the critical density for collapse δ_c , an important ingredient in excursion set based estimates of the mass function. They found that δ_c is lower for EDE models and hence for the same observed structure today ($z = 0, a = 1$), the structure must grow earlier in EDE models. They also noticed that, while there were more clusters at an earlier epoch in EDE than Λ CDM, the growth rate of structure from redshift 1 to 0 was slower in EDE than Λ CDM. Grossi & Springel (2008) performed numerical simulations to test the conclusions based on semi-analytic estimates. They found that no modification was required to the standard mass function formalism and the sensitivity of the halo mass function to EDE was much less than that predicted based on analytic estimates. Similar conclusions were reached by Francis et al. (2008). Fontanot et al. (2012) coupled dark matter simulations with semi-analytic models of gas physics to model galaxy formation in EDE scenarios and again found that galaxy properties could only weakly distinguish EDE from Λ CDM. More recently, Shi & Baugh (2016) performed more consistent simulations, which accounted for the fact that the EDE parameters that best fit the Planck data are different from those for Λ CDM and properly accounting for this changes the expansion history and in turn, the mass function estimates. They found that the cleanest signature of dark energy was on the shape of the power spectrum and this difference was elucidated only by adopting consistent linear theory initial conditions.

In this paper, we examine the differences between EDE and Λ CDM for the one-point PDF. On the scale of the plots in the earlier section, the differences between EDE and Λ CDM are barely perceptible by eye. To provide quantitative estimates

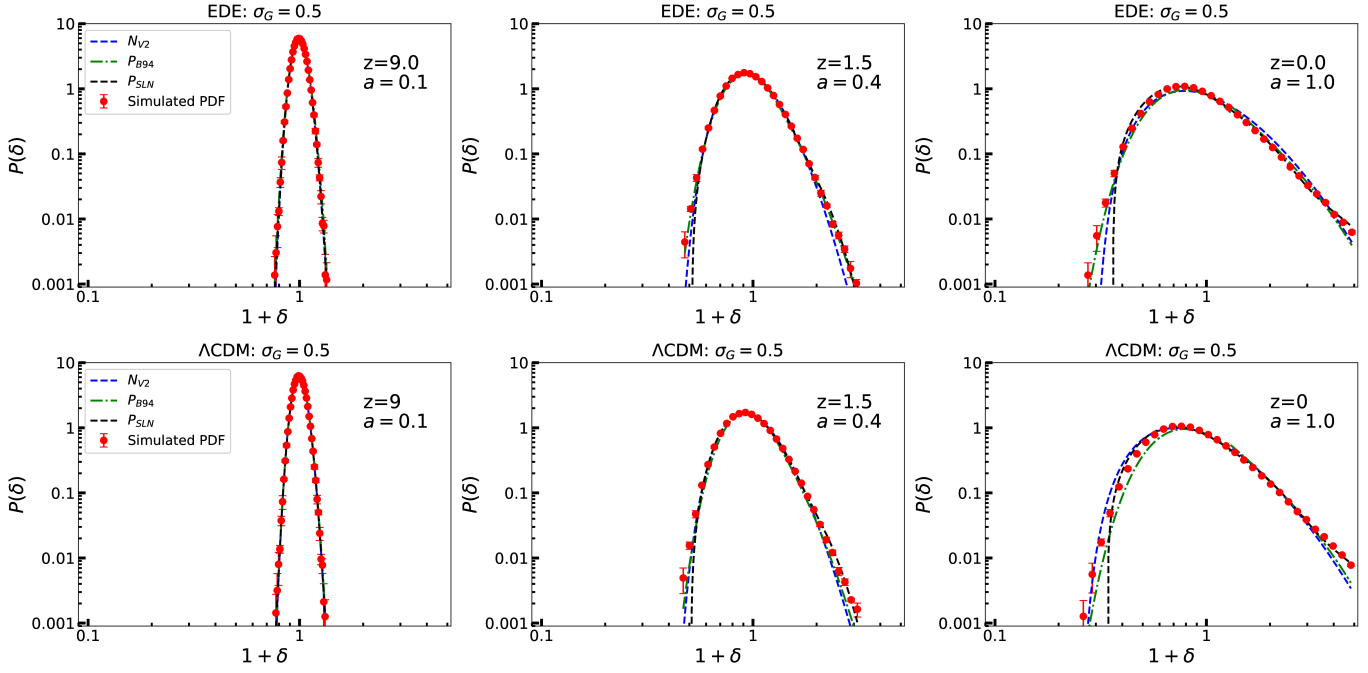


Figure 4. Variation of the one-point PDF with epoch. $P(\delta)$ vs. $(1 + \delta)$ for $\sigma_G = 0.5$ for the EDE and Λ CDM models at $a = 0.1, 0.4, 1$ ($z = 9, 1.5, 0$). Simulated PDFs (filled red circles) are compared with the predicted PDFs based on theory and N-body simulations. At $a = 0.1$, the Gaussian shape is retained, but non-Gaussian features appear at later epochs.

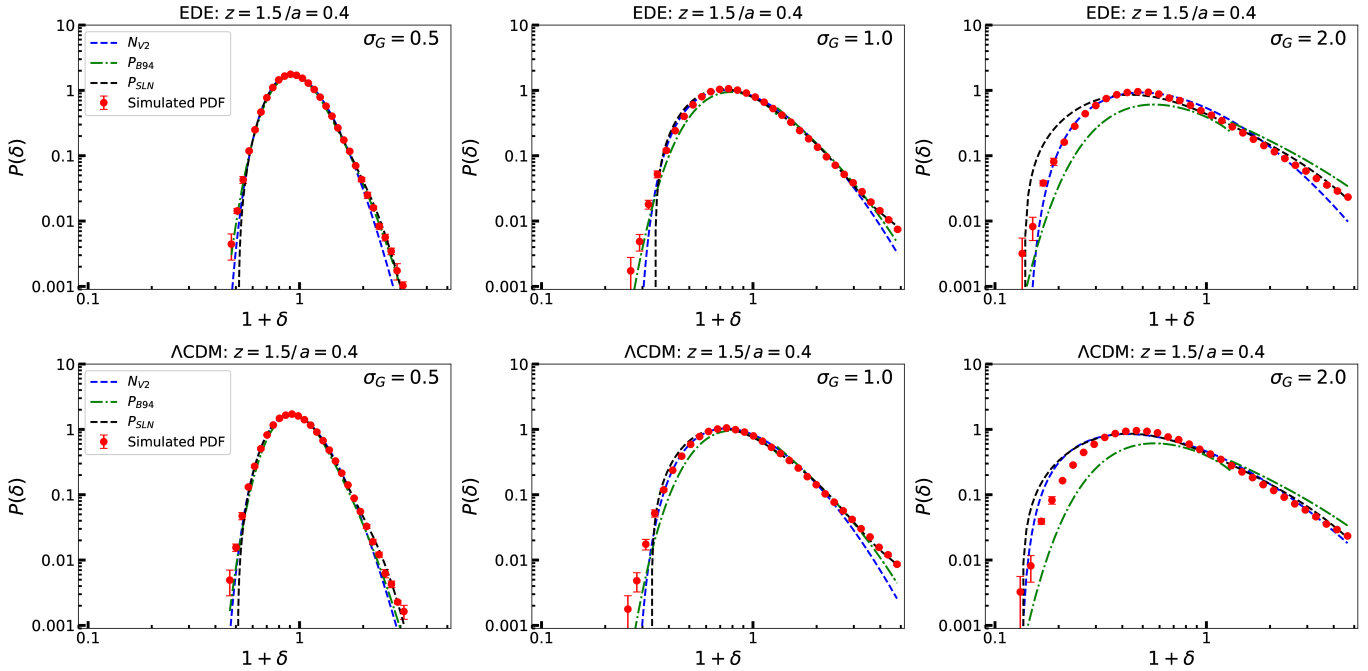


Figure 5. Dependence of one-point PDF on σ_G . $P(\delta)$ vs. $(1 + \delta)$ at $a = 0.4$ ($z = 1.5$) for the EDE and Λ CDM models for three values of $\sigma_G = 0.5, 1, 2$. Simulated PDFs (filled red circles) are compared with the predicted PDFs based on theory and N-body simulations. Higher σ_G distribution is more non-Gaussian at the same epoch.

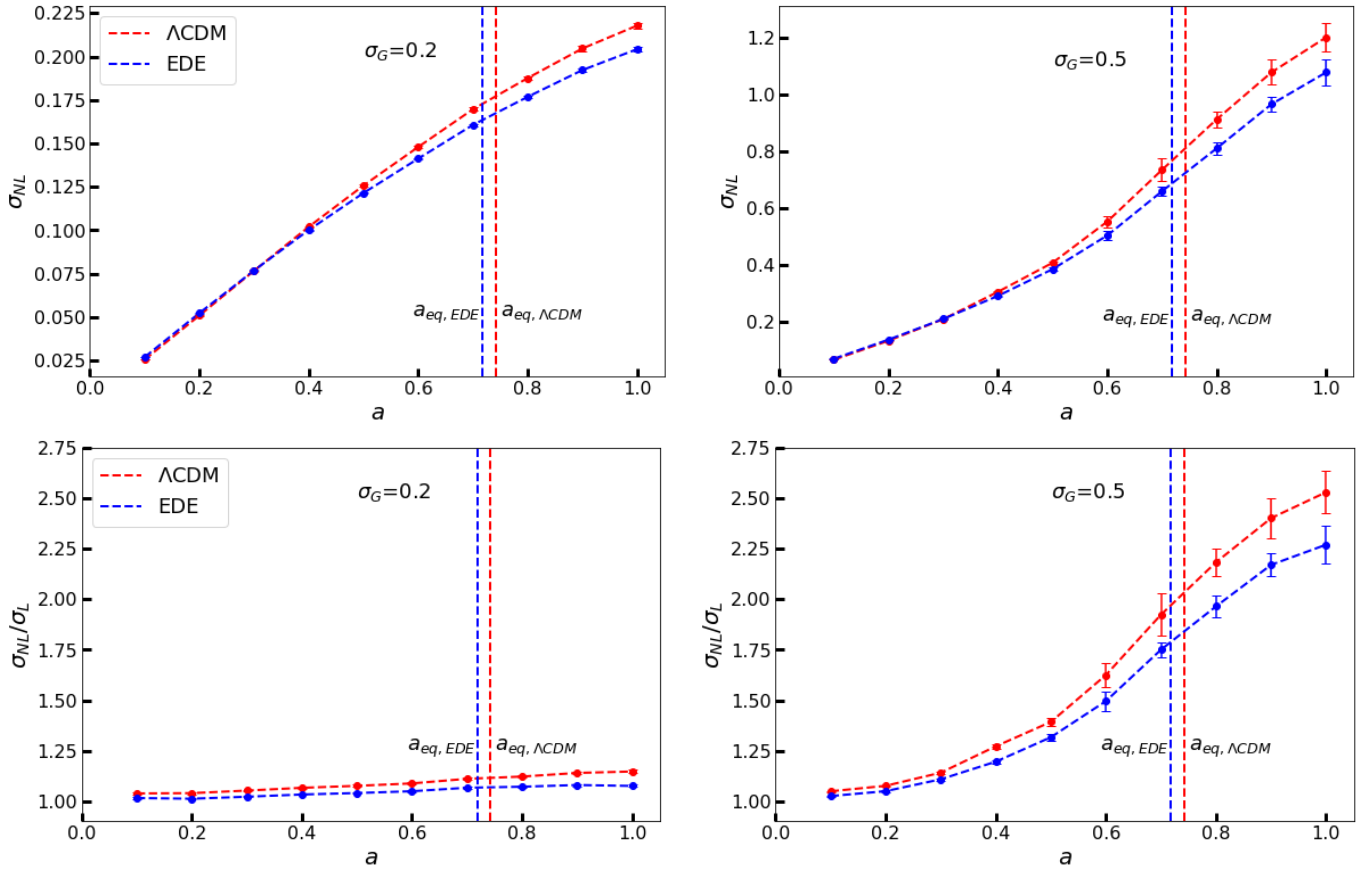


Figure 6. Width of the PDF (top panel) and scaled width (bottom panel) as a function of time. At very early epochs, the growth is linear and the scaled width is close to 1. For $\sigma_G = 0.2$, the evolution stays close to linear with the σ_{NL} deviating from the linear value by only 10%. For $\sigma_G = 0.5$, the growth is faster at early epochs but slows down the dark energy terms starts to dominate.

we compute the width of the PDF defined as standard deviation σ_{NL} :

$$\sigma_{NL} = \sqrt{\langle(\delta - \langle\delta\rangle)^2\rangle}, \quad -1 \leq \delta \leq 20. \quad (36)$$

The cut-off in the data was imposed at $\delta \leq 20$. In order to highlight the non-linear evolution, we also compute the scaled standard deviation: σ_{NL} divided by σ_L , where σ_L is defined in eq. (19). Figure 5 shows σ_{NL} (top) and its scaled value (bottom) for two values of $\sigma_G = 0.2$ and $\sigma_G = 0.5$ (the results for $\sigma_G = 1, 2$ are subject to the δ cut-off and are shown in appendix D). We evaluate the width at ten epochs between $a = 0.1$ and $a = 1$. The top panel shows that at early epochs, σ_{NL} grows linearly with a , for both scales, as expected, since the universe is matter dominated. For $\sigma_G = 0.2$, the fluctuations stay mostly linear, since σ_{NL} deviates only about 10% from its linear value even at late epochs. For $\sigma_G = 0.5$, the fluctuations become non-linear at late epochs. The growth rate (slope) increases from its linear value from $a \sim 0.4$ to $a \sim 0.8$, as is expected for non-linear evolution and it slows down after $a \sim 0.8$ due to the presence of the dark energy terms. For both scales considered here, the EDE and Λ CDM cases have the same qualitative trends. It is worth noting that the error bars, corresponding to deviations within realizations, are less than the separation between the two curves. This suggests that the evolution of σ_{NL} could potentially be a promising tool to distinguish between the EDE and dark energy scenarios. The fractional change between the two cases ($\sigma_{NL,EDE}/\sigma_{NL,\Lambda\text{CDM}} - 1$) at $a = 1$ is about 6% and 10% for the $\sigma_G = 0.2$ and $\sigma_G = 0.5$ respectively. Recently, Shin et al. (2017) also examined the differences of the matter density PDF for four different cosmologies. They too found that the simulated data showed deviations of about a few percent at $a = 1$.

We also considered higher moments for the weakly non-linear case of $\sigma_G = 0.2$ as a measure of the departure from non-Gaussianity. The skewness (third moment) defined in eq. (33) and the kurtosis (fourth moment) defined as,

$$\beta_2 = \frac{\langle(\delta - \mu)^4\rangle}{(\langle(\delta - \mu)^2\rangle)^2} \quad (37)$$

where μ is defined in eq. (31), are plotted in figure 5. At early epochs, the fluctuations have retained part of their initial Gaussianity and hence the skewness is near zero and kurtosis is near three as expected. Both skewness and kurtosis increase as the fluctuations pick up secondary non-Gaussianity. However, the error bars on the third and fourth moments are higher

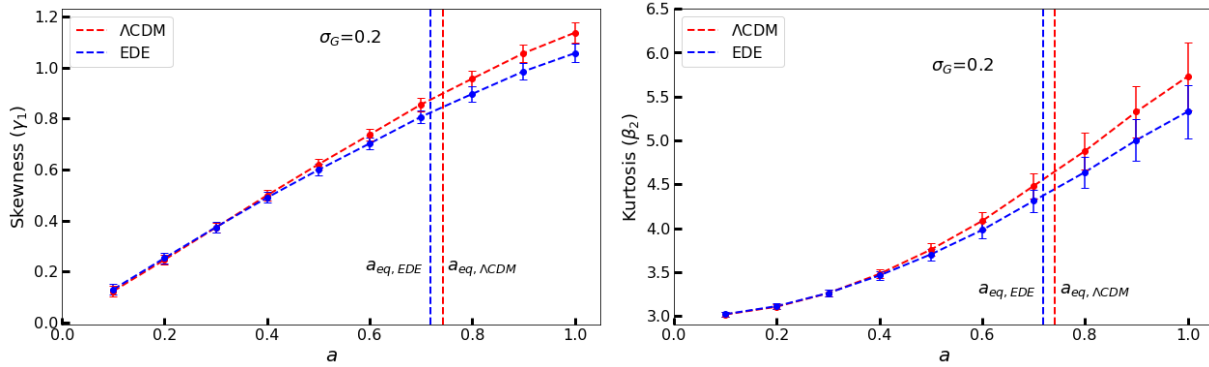


Figure 7. Skewness and kurtosis for $\sigma_G = 0.2$. At early epochs, the skewness is near zero and kurtosis is near 3, as is expected for a nearly Gaussian distribution. The departure from the gaussian form is higher at later epochs. The error bars for the higher moments are however, larger than those for the width, making it harder to use the higher moments to discriminate between models.

than those on the width σ_{NL} and slightly overlapping between the two cosmologies. For other scales, i.e., higher values of σ_G , the error bars on the skewness and kurtosis curves were too big and significantly overlapping to make any meaningful conclusions (and not shown here). Thus, the width of the PDF is the cleanest discriminant between the EDE and Λ CDM cosmologies

6 CONCLUSION

In this paper, we have considered the spherical collapse (SC) model for three cosmologies: pure matter (EdS), Λ CDM and one early dark energy (EDE) model, with non-interacting dark energy, but time-varying equation of state. There were three aims: (1) to compute the one-point PDF of the dark matter field and compare it with existing forms in the literature, (2) to understand the differences in the PDFs for EDE and Λ CDM models and (3) to examine if the density-velocity divergence relation (DVDR) derived by Nadkarni-Ghosh in N13 for constant w cosmologies can also be applied to the EDE model with time-varying w . To compare the PDFs, we considered three fitting functions: the theoretical estimate given by Bernardeau, referred to as B94 (Bernardeau 1994a), the skewed lognormal (SLN) form given by Colombi (1994) and the generalized normal distribution version 2 (\mathcal{N}_{v2}) recently proposed by Shin et al. 2017, based on numerical simulations. The initial distribution is assumed to be Gaussian, characterized by its comoving width σ_G . Three values were considered: $\sigma_G = 0.5, 1$ and 2 , which roughly correspond to a smoothing scale of $R_f = 15, 7$ and $3 h^{-1}$ Mpc for the BBKS power spectrum. The main conclusions are:

- For overdense regions the SLN distribution provides the best fit over the range of epochs from $a = 0.1$ to 1 , scales and the three cosmologies. For underdense regions, B94 and \mathcal{N}_{v2} perform better than SLN.
- For $\sigma_G = 0.2$ and $\sigma_G = 0.5$, we computed the standard deviation as a measure of the width of the PDF. These values of σ_G correspond to scales that are quasi-linear today and the observed differences between EDE and Λ CDM are of the order of ten percent. The error bars corresponding to deviations between realizations are smaller than this difference. Higher moments of the same distribution could not successfully discriminate between the two models. Thus, the standard deviation of the PDF could potentially be a future probe that provides constraints on EDE models. However, observational errors and uncertainty in the galaxy bias may prohibit this in practice.
- We computed the growth rate of perturbations in the linear and non-linear regime and found that as expected, growth is slower in the EDE models as compared to dark energy. Unlike the linear growth rate, which depends only on cosmological parameters, the non-linear growth rate is an instantaneous quantity i.e., it depends on the value of the density contrast δ at the epoch of interest and hence depends upon both the cosmological parameters and the initial conditions. To illustrate the implications of this dependence, we compared two cases with Zeldovich initial conditions: in the first case the two models have the same value of δ at $a = 0.001$, in the second case, they have the same value of the linearly evolved δ at $a = 1$. The difference in growth rates between the two models is more prominent in the first case than in the second. The difference in cosmological parameters (less value of Ω_m in EDE) is offset by a difference in initial conditions (higher value of initial δ in EDE).
- The form of the non-linear DVDR given by N13 was tested by examining the observed and predicted non-linear growth rates. The predicted growth rate was computed by combining the definition given by eq. (13) with the fitting form of Θ from N13, given by eq. (14). The error between observed and predicted rate is about 3%, confirming the validity of the N13 formula for EDE models. This suggests that the formula is robust, since it was derived based on constant w dark energy models.

Observationally, the one-point PDF is measured either using galaxy catalogs or using weak lensing convergence maps. The survey either measures positions of galaxies or observed ellipticities to compute a shear map. The density map is constructed using the Cloud-In-Cell (CIC) method which involves defining 2D or 3D cells in space, adding up the matter content in each cell and allotting a density to the cell depending upon the cell volume (for e.g., Bernardeau et al. 2002). This method introduces shot noise because of the finite cell size. This noise is often modelled by a Poisson distribution in the case of galaxies and a Gaussian in the case of the weak lensing convergence field (for e.g., Clerkin et al. 2017). In order to compare to data, the theoretically predicted continuous distribution has to be convolved with the noise distribution. In the case of galaxies, one needs to further account for the fact that they are biased tracers of the underlying dark matter distribution. Both these effects may introduce effects that are degenerate with the effect of changing cosmology.

The use of spherical dynamics to model the density one-point PDF is not new. Many investigations have coupled SC with some non-local techniques like perturbation theory, Edgeworth expansion, excursion sets, large deviation theory, path integral formalism, all of which account for the interaction between modes. However, in this analysis, we do not couple SC with any non-local scheme, which makes this a rather simple technique. Our study is motivated by the future goal of finding the one-point PDF for nontrivial cosmological models, particularly modified gravity or coupled dark energy. Complications arise in these situations because the dynamical variables are no longer just density and velocity. In the case of modified gravity, the ratio of the two gravitational potentials also becomes a dynamical variable (Nadkarni-Ghosh *et al.*, in preparation), whereas in the case of dark energy coupled to dark matter, the dark energy perturbation introduces an additional degree of freedom. Top-hats do not stay as top-hats (e.g., Dai et al. 2008; Borisov et al. 2012; Kopp et al. 2013) and defining the density PDF will involve taking a spatial average of the density for each initial perturbation. These issues can be better understood, with a simple scheme. Our work is perhaps most similar in spirit to that of Ohta et al. (2003) who obtained an analytical expression for the evolution equation of the PDF whereas, we follow the evolution of the PDF numerically. The new features of our analysis are the one-point PDF and the expression for the non-linear growth rate, which is derived from the density velocity divergence relation (eq. 16).

The SC model has numerous limitations. It is based on local dynamics. Thus, the two-point correlation functions and higher-order spatial statistics cannot be computed solely within this framework. Effect of the environment which induces tidal forces, rotation and accretion is ignored and so is mode-coupling and galaxy bias. Estimates based on perturbative schemes such as Lagrangian perturbation theory (Nadkarni-Ghosh & Chernoff 2011, 2013) or other approximate methods Monaco (2016) can account for some of the neglected effects. Nevertheless, the method presented in this paper allows for a quick comparative study of the evolution of the one-point PDF in various cosmologies.

7 ACKNOWLEDGEMENTS

SN would like to acknowledge the Department of Science and Technology (DST), Govt. of India for the grant no. (SR/WOS-A/PM-21/2018).

APPENDIX A: THE DYNAMICAL EQUATIONS

The physical system comprises of a perturbed sphere evolving in a background cosmology consisting of matter and dark energy with an equation of state w . The equation of state can be varying or time-dependent. The background evolution is completely described by a scale factor $a(t)$ given by eq. (1).

Let the origin be at the center of the inner sphere (perturbation) and \mathbf{r} and \mathbf{x} denote the physical and comoving coordinate of the outer edge of the sphere. Let $\mathbf{u} = \dot{\mathbf{x}}$ and δ denote the fractional overdensity. For pure matter cosmologies, it is possible to write down an analogous Friedmann equation by replacing the scale factor of the background by that of the perturbation with a different matter density parameter. However, the extension to other dark energy models is not obvious. Therefore, it is preferable to start with the equations of hydrodynamics, generalized to include dark energy. This set corresponds to the spherically symmetric, sub-horizon limit of the perturbed Einsteins' equations along with the conservation of the stress-energy tensor. In the weak-field, sub-horizon limit, for pure matter perturbations, the equations are:

$$\dot{\delta} = -(1 + \delta)\nabla_x \cdot \mathbf{u} \quad (\text{A1})$$

$$\dot{\mathbf{u}} + 2H\mathbf{u} = -\frac{1}{a^2}\nabla_x\psi \quad (\text{A2})$$

$$\nabla_x^2\psi = \frac{3}{2}a^2\Omega_m(a)H^2(a)\delta, \quad (\text{A3})$$

where the 'dot' refers to the total derivative w.r.t. cosmic time t ($d/dt = \partial/\partial t + \mathbf{u} \cdot \nabla_x$) and the partial spatial derivatives are with respect to the comoving coordinate \mathbf{x} . Taking divergence of eq. (A2), gives

$$\nabla_x \cdot \dot{\mathbf{u}} + 2H\nabla_x \cdot \mathbf{u} = -\frac{3}{2}H^2\Omega_m(a)\delta. \quad (\text{A4})$$

For the spherically symmetric system considered here, we have

$$\frac{d(\nabla_x \cdot \mathbf{u})}{dt} = \nabla_x \cdot \dot{\mathbf{u}} - \frac{(\nabla_x \cdot \mathbf{u})^2}{3} \quad (\text{A5})$$

Define the scaled velocity divergence as

$$\Theta = \frac{\nabla_x \cdot \mathbf{u}}{H}. \quad (\text{A6})$$

Equations (A1) and (A4) give the coupled system

$$\dot{\delta} = -H(1 + \delta)\Theta \quad (\text{A7})$$

$$\dot{\Theta} = -H \left[\frac{3}{2}\Omega_m(a)\delta + \left(2 + \frac{\dot{H}}{H^2} \right) \Theta + \frac{\Theta^2}{3} \right]. \quad (\text{A8})$$

Combining the two first order equations gives the second order system

$$\ddot{\delta} + 2H\dot{\delta} - \frac{4}{3}\frac{\dot{\delta}^2}{(1 + \delta)} - \frac{3}{2}H^2\Omega_m(a)\delta(1 + \delta) = 0. \quad (\text{A9})$$

Using $\ln a$ as the time variable instead of t ($d/dt = Hd/d\ln a$), gives the coupled system

$$\delta' = -(1 + \delta)\Theta \quad (\text{A10})$$

$$\Theta' = -\frac{3}{2}\Omega_m(a)\delta - \Theta \left(2 + \frac{H'}{H} \right) - \frac{\Theta^2}{3} \quad (\text{A11})$$

and the second order version

$$\delta'' + \left(2 + \frac{H'}{H} \right) \delta' - \frac{4}{3}\frac{\delta'^2}{(1 + \delta)} - \frac{3}{2}\Omega_m(a)\delta(1 + \delta) = 0. \quad (\text{A12})$$

For the dark energy cosmologies considered in this paper:

$$\frac{1}{H} \frac{dH}{d\ln a} = -\frac{3}{2}\Omega_m(a) - \frac{3}{2}(1 + w(a))\Omega_{de}(a). \quad (\text{A13})$$

For a flat universe: $\Omega_m(a) + \Omega_{de}(a) = 1$ at all epochs. So the factor

$$\left(2 + \frac{H'}{H} \right) = \frac{1}{2} [1 - 3w(a)\Omega_{de}(a)]. \quad (\text{A14})$$

This gives

$$\delta'' - \frac{4}{3}\frac{\delta'^2}{(1 + \delta)} + \frac{1}{2} [1 - 3w(a)\Omega_{de}(a)] \delta' - \frac{3}{2}\Omega_m(a)\delta(1 + \delta) = 0. \quad (\text{A15})$$

This second order non-linear equation for the evolution of δ has been considered in the past by Fosalba & Gaztanaga (1998) as well as Ohta et al. (2003), but applied to pure matter cosmologies.

Model	σ_G	a	α	κ	ξ
EdS	0.5	0.1	0.049	-0.086	0.9999
		0.4	0.198	-0.313	0.9998
		1.0	0.518	-0.661	1.042
	1.0	0.1	0.098	-0.156	1.0001
		0.4	0.392	-0.564	1.001
		1.0	0.821	-0.921	1.018
	2.0	0.1	0.197	-0.308	0.999
		0.4	0.6105	-0.790	0.941
		1.0	0.897	-1.206	0.8008
Λ CDM	0.5	0.1	0.064	-0.108	0.999
		0.4	0.254	-0.389	1.000
		1.0	0.504	-0.670	0.988
	1.0	0.1	0.128	-0.201	1.001
		0.4	0.476	-0.645	0.993
		1.0	0.832	-0.948	0.990
	2.0	0.1	0.256	-0.389	0.9998
		0.4	0.766	-0.987	0.904
		1.0	0.848	-1.223	0.743
EDE	0.5	0.1	0.067	-0.113	0.999
		0.4	0.245	-0.377	1.000
		1.0	0.539	-0.671	1.078
	1.0	0.1	0.135	-0.213	1.001
		0.4	0.495	-0.665	1.008
		1.0	0.728	-0.867	0.977
	2.0	0.1	0.269	-0.406	0.999
		0.4	0.612	-0.840	0.863
		1.0	0.851	-1.134	0.812

Table B1. Values of the parameters α , κ and ξ for best fitted \mathcal{N}_{v2} distribution:

APPENDIX B: BEST FIT PARAMETERS FOR THE \mathcal{N}_{v2} DISTRIBUTION FOR THE THREE COSMOLOGIES.

Model	σ_G	a	Underdense			Overdense		
			B94	SLN	\mathcal{N}_{v2}	B94	SLN	\mathcal{N}_{v2}
EdS	0.5	0.1	0.088	0.095	0.089	0.088	0.095	0.092
		0.4	0.194	0.106	0.251	0.194	0.106	0.247
		1.0	0.194	0.163	0.228	0.194	0.06	0.228
	1.0	0.1	0.179	0.089	0.194	0.168	0.045	0.074
		0.4	0.384	0.120	0.229	0.265	0.057	0.347
		1.0	0.572	0.215	0.179	0.380	0.173	0.217
	2.0	0.1	0.193	0.271	0.230	0.176	0.081	0.258
		0.4	0.516	0.818	0.350	0.238	0.125	0.261
		1.0	0.714	2.850	0.520	0.526	0.136	0.347
Λ CDM	0.5	0.1	0.164	0.139	0.154	0.189	0.107	0.122
		0.4	0.352	0.173	0.203	0.281	0.142	0.328
		1.0	0.420	0.249	0.472	0.340	0.230	0.350
	1.0	0.1	0.177	0.129	0.169	0.199	0.062	0.121
		0.4	0.467	0.378	0.258	0.196	0.062	0.31
		1.0	0.578	1.188	1.068	0.383	0.123	0.281
	2.0	0.1	0.263	0.273	0.236	0.216	0.120	0.098
		0.4	0.574	1.534	0.756	0.380	0.130	0.120
		1.0	0.720	2.608	1.938	1.420	0.134	0.275
EDE	0.5	0.1	0.146	0.131	0.188	0.095	0.202	0.179
		0.4	0.164	0.179	0.216	0.130	0.131	0.232
		1.0	0.239	0.194	0.248	0.171	0.078	0.227
	1.0	0.1	0.087	0.161	0.192	0.168	0.038	0.119
		0.4	0.345	0.233	0.216	0.166	0.059	0.236
		1.0	0.489	0.428	0.362	0.373	0.125	0.212
	2.0	0.1	0.188	0.296	0.264	0.160	0.129	0.242
		0.4	0.530	1.46	0.255	0.390	0.131	0.274
		1.0	0.689	2.51	0.23	1.420	0.132	0.336

Table C1. Error of the fitting to different analytic forms of distribution function. We have calculated the error of fitting separately for underdense and overdense region:

Model	a	B94	SLN	\mathcal{N}_{v2}
EdS	0.1	0.148	0.112	0.156
	0.4	0.298	0.222	0.281
	1.0	0.43	0.538	0.287
Λ CDM	0.1	0.201	0.138	0.150
	0.4	0.375	0.403	0.329
	1.0	0.638	0.755	0.731
EDE	0.1	0.141	0.159	0.197
	0.4	0.287	0.365	0.238
	1.0	0.563	0.578	0.268

Table C2. Error of the fitting to different analytic forms of distribution function at different epoch averaged over σ_G and full density range

APPENDIX C: ERROR TABLES FOR THE THREE FITTING FUNCTIONS CONSIDERED HERE.

APPENDIX D: WIDTH OF THE ONE-POINT PDF

The upper panel of figure D shows the variation of σ_{NL} as a function of a ($a = 0.1, 0.4, 1$). It is clear that for all values of σ_G the width of the PDF increases with time. Between $a = 0.1$ and $a = 0.4$, the rate of increase is higher for higher σ_G , which is expected because the non-linear growth rate is higher for higher δ values. From $a = 0.4$ to $a = 1$, there is an apparent slow-down in the growth rate for $\sigma_G = 1, 2$. While slow down is expected at higher epochs due to the presence of dark energy, the one observed slow down is an artefact of the cut-off in δ imposed in the construction of the PDF. For $\sigma_G = 2$, that the change (increase) in σ_{NL} from $a = 0.4$ to $a = 1$ was higher when the cut-off δ was increased from 5 (plot not shown) to 20 (this plot).

Model	σ_G	B94	SLN	\mathcal{N}_{v2}
EdS	0.5	0.158	0.104	0.189
	1.0	0.324	0.116	0.206
	2.0	0.393	0.713	0.327
Λ CDM	0.5	0.291	0.173	0.271
	1.0	0.333	0.323	0.367
	2.0	0.595	0.799	0.570
EDE	0.5	0.157	0.152	0.215
	1.0	0.271	0.174	0.236
	2.0	0.563	0.776	0.267

Table C3. Error of the fitting to different analytic forms of distribution function at different σ_G averaged over epochs and full density range

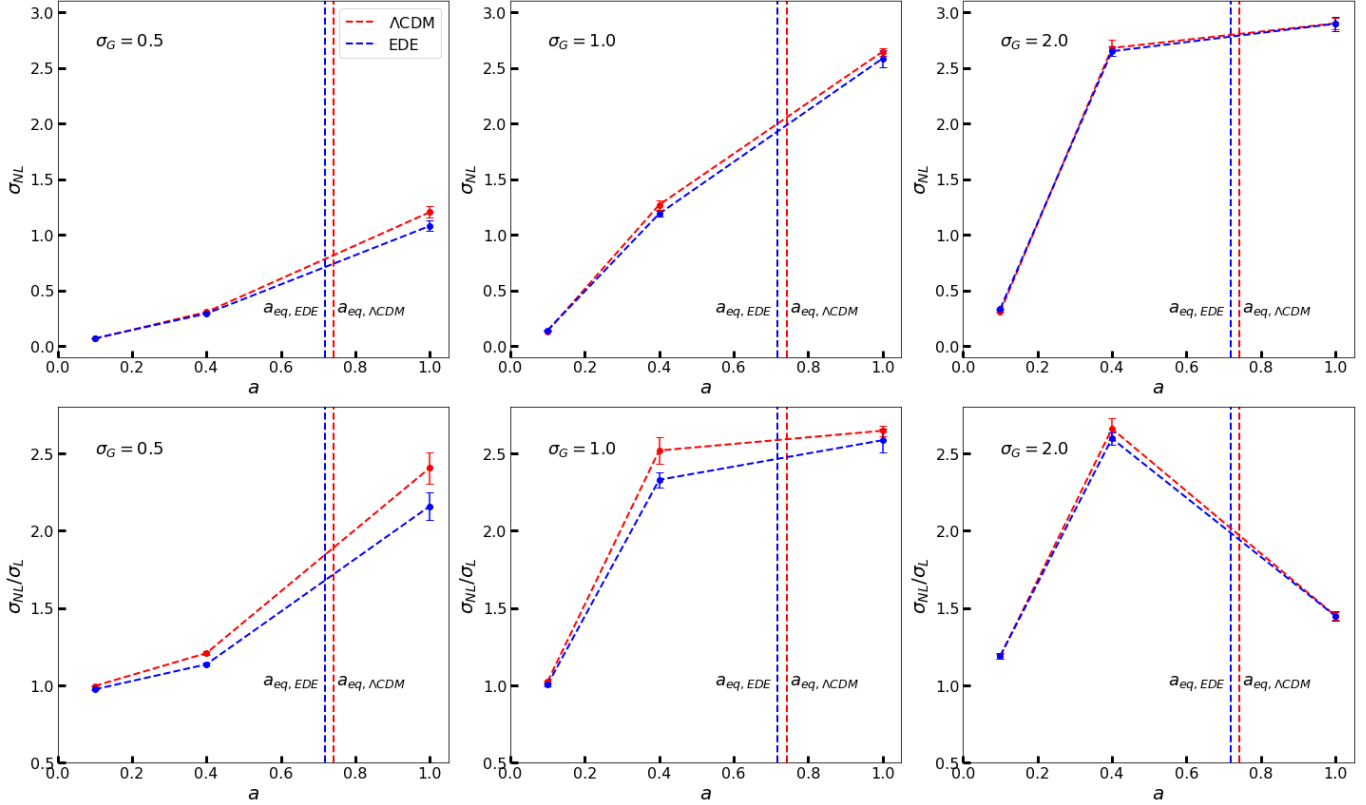


Figure D1. Width of the PDF (top panel) and scaled width (bottom panel) as a function of time. The flattening for $\sigma_G = 2$ is an effect of a finite cutoff imposed on the δ values in computing the PDF.

REFERENCES

- Abramo L. R., Batista R. C., Liberato L., Rosenfeld R., 2009, *Physical Review D*, 79, 023516
 Bartelmann M., Doran M., Wetterich C., 2006, *Astronomy and Astrophysics*, 454, 27
 Bel J. et al., 2016, *Astronomy and Astrophysics*, 588, A51
 Bernardeau F., 1992, *The Astrophysical Journal*, 390, L61
 Bernardeau F., 1994a, *Astronomy and Astrophysics*, 291, 697
 Bernardeau F., 1994b, *The Astrophysical Journal*, 433, 1
 Bernardeau F., Chodorowski M. J., okas E. L., Stompor R., Kudlicki A., 1999, *Monthly Notices of the Royal Astronomical Society*, 309, 543
 Bernardeau F., Codis S., Pichon C., 2015, *Monthly Notices of the Royal Astronomical Society*, 449, L105
 Bernardeau F., Colombi S., Gaztaaga E., Scoccimarro R., 2002, *Physics Reports*, 367, 1
 Bernardeau F., Kofman L., 1995, *The Astrophysical Journal*, 443, 479
 Bernardeau F., Pichon C., Codis S., 2014, *Physical Review D*, 90, 103519

- Bernardeau F., Reimberg P., 2016, *Physical Review D*, 94, 063520
- Bilicki M., Chodorowski M. J., 2008, *Monthly Notices of the Royal Astronomical Society*, 391, 1796
- Borisov A., Jain B., Zhang P., 2012, *Physical Review D*, 85, 63518
- Clerkin L. et al., 2017, *Monthly Notices of the Royal Astronomical Society*, 466, 1444
- Codis S., Pichon C., Bernardeau F., Uhlemann C., Prunet S., 2016, *Monthly Notices of the Royal Astronomical Society*, 460, 1549
- Coles P., Jones B., 1991, *Monthly Notices of the Royal Astronomical Society*, 248, 1
- Coles P., Melott A. L., Shandarin S. F., 1993, *Monthly Notices of the Royal Astronomical Society*, 260, 765
- Colombi S., 1994, *The Astrophysical Journal*, 435, 536
- Colombi S., Bernardeau F., Bouchet F. R., Hernquist L., 1997, *Monthly Notices of the Royal Astronomical Society*, 287, 241
- Colombi S., Szapudi I., Jenkins A., Colberg J., 2000, *Monthly Notices of the Royal Astronomical Society*, 313, 711
- Dai D.-C., Maor I., Starkman G., 2008, *Physical Review D*, 77, 64016
- Dodelson S., 2003, *Modern Cosmology*, 2nd edn. Academic Press
- Doran M., Robbers G., 2006, *Journal of Cosmology and Astro-Particle Physics*, 2006, 026
- Fontanot F., Springel V., Angulo R. E., Henriques B., 2012, *Monthly Notices of the Royal Astronomical Society*, 426, 2335
- Fosalba P., Gaztanaga E., 1998, *Monthly Notices of the Royal Astronomical Society*, 301, 535
- Francis M. J., Lewis G. F., Linder E. V., 2008, 0808.2840, *mon.Not.Roy.Astron.Soc.*394:605-614,2008
- Gaztañaga E., Fosalba P., Elizalde E., 2000, *The Astrophysical Journal*, 539, 522
- Grossi M., Springel V., 2008, 0809.3404
- Gruen D. et al., 2018, *Physical Review D*, 98, 023507
- Hilbert S., Hartlap J., Schneider P., 2011, *Astronomy and Astrophysics*, 536, A85
- Hubble E., 1934, *The Astrophysical Journal*, 79, 8
- Hurtado-Gil L., Martinez V. J., Arnalte-Mur P., Pons-Bordera M.-J., Pareja-Flores C., Paredes S., 2017, *Astronomy and Astrophysics*, 601, A40
- Ivanov M. M., Kaurov A. A., Sibiryakov S., 2019, *Journal of Cosmology and Astro-Particle Physics*, 2019, 009
- Jennings E., Baugh C. M., Angulo R. E., Pascoli S., 2010, *Monthly Notices of the Royal Astronomical Society*, 401, 2181
- Juszkiewicz R., Weinberg D. H., Amsterdamski P., Chodorowski M., Bouchet F., 1995, *Astrophysical Journal*, 442, 39
- Kitaura F.-S., Heß S., 2013, *Monthly Notices of the Royal Astronomical Society*, 435, L78
- Klypin A., Prada F., Betancort-Rijo J., Albareti F. D., 2018, *Monthly Notices of the Royal Astronomical Society*, 481, 4588
- Kofman L., 1993, arXiv e-prints, astro
- Kofman L., Bertschinger E., Gelb J. M., Nusser A., Dekel A., 1994, *The Astrophysical Journal*, 420, 44
- Kopp M., Appleby S. A., Achitouv I., Weller J., 2013, *Physical Review D*, 88, 084015
- Kudlicki A., Chodorowski M., Plewa T., Ryczka M., 2000, *Monthly Notices of the Royal Astronomical Society*, 316, 464
- Lahav O., Itoh M., Inagaki S., Suto Y., 1993, *The Astrophysical Journal*, 402, 387
- Lam T. Y., Sheth R. K., 2008a, *Monthly Notices of the Royal Astronomical Society*, 389, 1249
- Lam T. Y., Sheth R. K., 2008b, *Monthly Notices of the Royal Astronomical Society*, 386, 407
- Lima J. A. S., Zanchin V., Brandenberger R., 1997, *Monthly Notices of the Royal Astronomical Society*, 291, L1
- Linder E. V., 2005, *Physical Review D*, 72, 43529
- Liu J., Hill J. C., Sherwin B. D., Petri A., Bhm V., Haiman Z., 2016, *Physical Review D*, 94, 103501
- Monaco P., 1999, *Observational Cosmology: The Development of Galaxy Systems*, 176, 186
- Monaco P., 2016, *Galaxies*, 4, 53
- Nadkarni-Ghosh S., 2013, *Monthly Notices of the Royal Astronomical Society*, 428, 1166
- Nadkarni-Ghosh S., Chernoff D. F., 2011, *Monthly Notices of the Royal Astronomical Society*, 410, 1454
- Nadkarni-Ghosh S., Chernoff D. F., 2013, *Monthly Notices of the Royal Astronomical Society*, 431, 799
- Nadkarni-Ghosh S., Singhal A., 2016, *Monthly Notices of the Royal Astronomical Society*, 457, 2773
- Neyman J., 1962, *Problems of Extra-Galactic Research*, 15, 294
- Ohta Y., Kayo I., Taruya A., 2003, *The Astrophysical Journal*, 589, 1
- Ohta Y., Kayo I., Taruya A., 2004, *The Astrophysical Journal*, 608, 647
- Pace F., Meyer S., Bartelmann M., 2017, *Journal of Cosmology and Astro-Particle Physics*, 10, 040
- Pace F., Waizmann J.-C., Bartelmann M., 2010, *Monthly Notices of the Royal Astronomical Society*, 406, 1865
- Patton K., Blazek J., Honscheid K., Huff E., Melchior P., Ross A. J., Suchyta E., 2017, *Monthly Notices of the Royal Astronomical Society*, 472, 439
- Peebles P. J. E., 1980, *The large-scale structure of the universe*. Princeton University Press
- Reimberg P., Bernardeau F., 2018, *Physical Review D*, 97, 023524
- Repp A., Szapudi I., 2018, *Monthly Notices of the Royal Astronomical Society*, 473, 3598
- Russell E., Pycke J.-R., 2017, *The Astrophysical Journal*, 835, 69
- Saslaw W. C., Hamilton A. J. S., 1984, *The Astrophysical Journal*, 276, 13

- Scott E. L., 1962, *Problems of Extra-Galactic Research*, 15, 269
- Shi D., Baugh C. M., 2016, *Monthly Notices of the Royal Astronomical Society*, 459, 3540
- Shin J., Kim J., Pichon C., Jeong D., Park C., 2017, *ArXiv e-prints*, 1705, arXiv:1705.06863
- Suto Y., Itoh M., Inagaki S., 1990, *The Astrophysical Journal*, 350, 492
- Szapudi I., Colombi S., Jenkins A., Colberg J., 2000, *Monthly Notices of the Royal Astronomical Society*, 313, 725
- Szapudi I., Pan J., 2004, *The Astrophysical Journal*, 602, 26
- Taruya A., Takada M., Hamana T., Kayo I., Futamase T., 2002, *The Astrophysical Journal*, 571, 638
- Taylor A. N., Watts P. I. R., 2000, *Monthly Notices of the Royal Astronomical Society*, 314, 92
- Ueda H., Yokoyama J., 1996, *Monthly Notices of the Royal Astronomical Society*, 280, 754
- Uhlemann C., Codis S., Hahn O., Pichon C., Bernardeau F., 2017, *Monthly Notices of the Royal Astronomical Society*, 469, 2481
- Uhlemann C., Codis S., Pichon C., Bernardeau F., Reimberg P., 2016, *Monthly Notices of the Royal Astronomical Society*, 460, 1529
- Uhlemann C., Pichon C., Codis S., L'Huillier B., Kim J., Bernardeau F., Park C., Prunet S., 2018, *Monthly Notices of the Royal Astronomical Society*, 477, 2772
- Valageas P., 1998, *Astronomy and Astrophysics*, 337, 655
- Valageas P., 2001, *Astronomy and Astrophysics*, 379, 8
- Valageas P., 2002a, *Astronomy and Astrophysics*, 382, 412
- Valageas P., 2002b, *Astronomy and Astrophysics*, 382, 431
- Valageas P., 2002c, *Astronomy and Astrophysics*, 382, 450
- Valageas P., 2002d, *Astronomy and Astrophysics*, 382, 477
- Valageas P., Munshi D., 2004, *Monthly Notices of the Royal Astronomical Society*, 354, 1146
- Wetterich C., 2004, *Physics Letters B*, 594, 17
- Wild V. et al., 2005, *Monthly Notices of the Royal Astronomical Society*, 356, 247
- Xavier H. S., Abdalla F. B., Joachimi B., 2016, *Monthly Notices of the Royal Astronomical Society*, 459, 3693
- Zeldovich Y. B., 1970, *Astronomy and Astrophysics*, 5, 84